

NOTES AND CORRESPONDENCE

On Wind, Convection, and SST Variations in the Northeastern Tropical Pacific Associated with the Madden–Julian Oscillation*

SOLINE BIELLI AND DENNIS L. HARTMANN

Department of Atmospheric Sciences, University of Washington, Seattle, Washington

10 March 2003 and 27 March 2004

ABSTRACT

Lagged maximum covariance analysis (LMCA) is used to examine the intraseasonal variability of zonal wind, sea surface temperature (SST), and outgoing longwave radiation (OLR) in the northeastern tropical Pacific Ocean during Northern Hemisphere summertime. The analysis shows a strong temporal asymmetry in that wind and convection anomalies lead to SST anomalies, but SST anomalies are not followed by comparably strong wind and convection anomalies. This suggests that SST anomalies associated with the MJO in the northeastern tropical Pacific are largely subject to atmospheric variability.

1. Introduction

The Madden–Julian oscillation (MJO) exists throughout the year (Madden and Julian 1994), and generally propagates eastward across the Indian Ocean to the Pacific Ocean (e.g., Weickmann 1983; Weickmann et al. 1985; Knutson et al. 1986). A local amplification of the MJO occurs over the eastern Pacific Ocean near Central America during Northern Hemisphere (NH) summer, where a pool of warm sea surface temperature (SST) is located (e.g., Maloney and Hartmann 2000a). In the northeastern tropical Pacific, westerly 850-mb zonal wind anomalies are associated with periods of enhanced convection, and easterly anomalies are accompanied by periods of suppressed convection. During the period when MJO wind anomalies are westerly at 850 mb, hurricanes are much more likely to develop in the East Pacific and the Gulf of Mexico (Maloney and Hartmann 1998, 2000a, 2000b).

In this note, we attempt to address the causal relationships among wind, convection, and SST variations associated with the MJO in the East Pacific. Maloney and Kiehl (2002a) used an eight-phase compositing analysis based on 31 strong MJO events to study the

relationships among wind, outgoing longwave radiation (OLR) and SST variations associated with the MJO in the tropical Pacific. They concluded that the highest SST leads convection by about 10 days. The eight-phase compositing technique used by Maloney and Kiehl (2002a) contains an implied assumption of periodicity, and, indeed, the negative and positive phases of the oscillation are nearly equal and opposite by construction. If the phenomenon is assumed periodic, then phase lags cannot be used to infer causality. Maloney and Kiehl (2002a) emphasized that the warmest water precedes the convection, implying that warm water enhances the convection anomalies on the MJO time scale. Their energy budget results suggest that the convection is important in cooling the ocean, through enhanced evaporation and reduced surface insolation.

In this note, we use a linear regression analysis using all of the data to investigate the time-lagged relationships between wind, OLR, and SST. The approach taken here is closer to a linear impulse response analysis and does not contain an assumption of periodicity. We hypothesize that lagged covariance can be a good indicator of whether winds drive SST anomalies or SST anomalies drive convection and winds. The analysis of lagged covariance will be examined by a singular value decomposition (SVD) of the lagged covariance matrices, which we will call the lagged maximum covariance analysis (LMCA). Data from May to November that have only been high-pass filtered to remove seasonal and longer time scales are used. This analysis shows a significant temporal asymmetry between convection, winds, and SST, which suggests that the effect of con-

* Joint Institute for the Study of the Atmosphere and Ocean Contribution Number 999.

Corresponding author address: Dr. Soline Bielli, Université du Québec à Montréal–Ouranos, 550 rue Sherbrooke Ouest, Montréal, QC H3A 1B9, Canada.
E-mail: biellisoline@uqam.ca

vection on SST is more important than the effect of SST on convection.

2. Data description and analysis

The 850-mb zonal wind, 200-mb zonal wind, and the SST data used in this study come from the European Centre for Medium-Range Weather Forecasts (ECMWF) gridded reanalysis data ($2.5^\circ \times 2.5^\circ$) for the years 1979–93 (Gibson et al. 1997). Data were available every 6 h and were averaged daily. Anomaly winds were calculated by subtracting the annual cycle from the daily mean data. The annual cycle was constructed by averaging values on individual days of the year over the 15 yr of interest and was smoothed using a box filter of three points. Additional low-frequency signals were removed using a Butterworth Filter with a cutoff period of 90 days. Applying an additional low-pass filter with a cutoff near 5 days did not produce significant differences in either shape or explained covariance, compared to only high-pass-filtered data.

The National Oceanic and Atmospheric Administration (NOAA) OLR product ($2.5^\circ \times 2.5^\circ$) for 1979–93 was used (Liebmann and Smith 1996). The same preprocessing was applied to the wind and OLR data. Data only from the period 1 May–30 November were used, when the MJO is enhanced over the eastern tropical Pacific Ocean.

The basic analysis method is SVD of lagged covariance matrices [see Bretherton et al. (1992) and Wallace et al. (1992) for a detailed description of SVD of covariance matrices]. Since SVD is a general operation on any matrix, we follow von Storch and Zwiers (1999) in using the more specifically descriptive term maximum covariance analysis (MCA), which in our case is applied to a lagged covariance matrix. LMCA is used here to examine the temporal and spatial relationships among winds, SST, and OLR during the season of enhanced MJO activity in the eastern tropical Pacific.

As an input to LMCA analyses, we computed the temporal covariance matrix between pairs of variables for time lags from 0- to 21-day intervals (with a 3-day increment) for each grid point. The significance of the linear relationship between the two fields can be evaluated by calculating the normalized root-mean-square covariance (RMSC) defined as follows:

$$\text{RMSC} = \frac{\left[\sum_{i=1}^M \sum_{j=i}^L (\bar{x}_i \bar{y}_j)^2 \right]^{1/2}}{\left(\sum_{i=1}^M \bar{x}_i^2 \right) \left(\sum_{j=1}^L \bar{y}_j^2 \right)}, \quad (2.1)$$

where x and y are the two datasets used in the MCA. The RMSC is on the order of 0.1 for well-correlated fields (Wallace et al. 1992).

The analysis produces two singular vectors for each mode. One singular vector is associated with a field at

a later time (with a lag of 0, 3, 6, 9 . . . 21 days), and the other singular vector is associated with the other field at the earlier time. The singular vectors for zero lag are identical to each other and to the classic empirical orthogonal function (EOF) when doing MCA of the field with itself. All the results have been dimensionalized so that the singular vectors have the units of the fields that they represent, which are m s^{-1} for the wind, W m^{-2} for the OLR, and K for SST. We show only the heterogeneous maps, which show the amplitude associated with the covariance between two fields (Bretherton et al. 1992).

LMCA analysis was performed on two different domains to try to assess the sensitivity of the analysis to the choice of the domain. The first domain considered includes the region from 10°S to 30°N and from 180° to 60°W (hereafter the large domain). The second analysis was performed on a smaller domain (hereafter the small domain) and is confined within the region of maximum variation of the MJO, that is, from 0° to 30°N and from 130° to 80°W . Results will be shown for the large domain. The structures are very similar for the two domains, which shows robustness with respect to changes in the domain boundaries. Using a smaller domain does, however, increase the fraction of covariance explained by the leading mode of the LMCA analysis, as one would expect. This increase is particularly large for the OLR field, which contains large amounts of high-frequency noise.

Figure 1 (left) shows the mean and standard deviation of 850-mb zonal wind for May–November averaged over the period 1979–93. Plots are based on unfiltered daily averages of ECMWF reanalysis data. During this period, the mean winds are mainly easterly in the region of interest. The maximum variability, which is greater than 4 m s^{-1} , occurs near 12°N and between 120° and 90°W , which corresponds to the region where the MJO signal is largest and where a maximum tropical cyclone development occurs.

Figure 1 (right) shows the mean and standard deviation of OLR daily data for the same period as the zonal wind. The mean OLR shows a convective region (OLR less than 240 W m^{-2}) between 10° and 15°N associated with the position of ITCZ during summertime. The maximum variation occurs along the same latitude line, and especially where the 850-mb zonal winds show their maximum variability. The maximum standard deviation of 45 W m^{-2} for OLR appears to be just east of the maximum of 5 m s^{-1} for the 850-mb wind.

3. Results

a. Zonal wind at 850 and 200 mb

In the interest of economy, the results of LMCA of zonal wind with itself will not be shown, particularly since the conclusions are similar to those drawn by previous investigators. LMCA of the 850-mb zonal wind

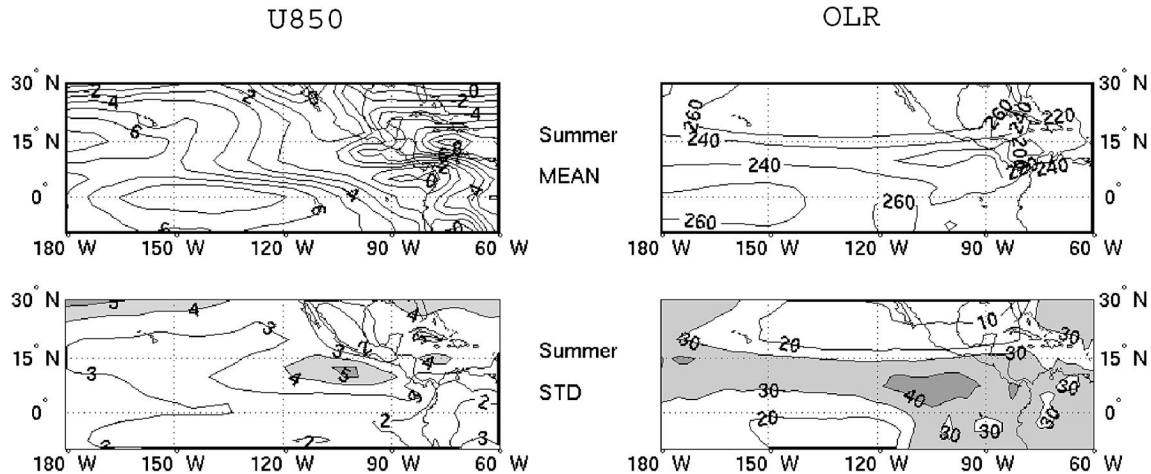


FIG. 1. (left) Mean and standard deviation of the 850-mb zonal wind for the period May–Nov and from 1979 to 1993 derived from the ECMWF reanalysis and based on daily mean values. Mean positive values and standard deviation values greater than 4 m s^{-1} are shaded. (right) Same as left, but for the OLR.

shows evidence of eastward propagation in that the significant amplitudes move eastward with increasing time. The RMSC of the leading mode of the LMCA of 850-mb zonal wind is of the order of 0.1 and decreases with an increased time lag. It is larger for the small domain for small lags but about the same for both domains for 6- and 9-day lags. The fraction of explained covariance varies from 12% to 23% with larger values for 3- and 6-day lags. The fraction increases by a factor of almost 2 for the small domain compared to the large domain.

The leading mode of LMCA analysis for the 850-mb zonal wind with itself at zero lag is very similar to the first EOF computed on a different domain and described by Maloney and Hartmann (2001) with a maximum of about 2 m s^{-1} located around 12°N and 100°W . As the lag is increased, the leading mode exhibits a decrease of amplitude, and earlier times show westerly anomalies extending farther to the west, suggesting eastward propagation of the signal.

The first singular vectors for the zero-lag LMCA of 850-mb zonal wind with 200-mb zonal wind show that the 850-mb westerly jet is associated with a jet of the opposite sign in the upper level and mainly south of the equator, as previously observed by Maloney and Hartmann (2000a). The fraction of covariance explained by the leading mode varies between 17% and 22%, depending on the time lag, again with maximum values for 3- and 6-day lags. The RMSC values are of the same order as those calculated for the 850-mb zonal wind.

To summarize, lagged covariance analysis of 850- and 200-mb zonal wind gives results consistent with previous EOF and compositing analysis of the structure and evolution of the MJO variability in the eastern tropical Pacific during NH summer. The explained covariance is around 20% for the larger domain and the RMSC is around 0.1 for lags up to a week.

b. 850-mb zonal wind and OLR

1) 850-MB ZONAL WIND LEADS OLR

Figure 2 shows the leading LMCA mode of the OLR with the 850-mb zonal wind, in which the wind leads the OLR by 0, 3, 6, and 9 days. The fraction of covariance explained by the leading mode is around 12% (it doubles for the small domain). The RMSC is slightly weaker than 0.1 but still remains of the same order of magnitude, showing a relatively good covariance between the 850-mb zonal wind and the OLR patterns for all of the time lags.

Figure 2 (top) shows that the region of maximum convection that is located near 15°N and 100°W is associated with maximum westerly wind anomalies, similar to what has been shown by Maloney and Kiehl (2002a) during phase 5 and 6 of their MJO composite. Along the east coast of Central America, a small region of suppressed convection can be seen at all nonzero lags, near 10°N and 80°W . The positions of the regions of enhanced and suppressed convection are consistent with the locations of the maximum and minimum precipitation anomalies shown in Maloney and Hartmann (2000a). As the temporal lag between the wind and OLR is increased, the region of enhanced convection progressively decreases in intensity from a maximum of about -15 W m^{-2} to -5 W m^{-2} , 6 days after the maximum of westerly winds. By day 9, this region has been replaced by a positive OLR anomaly and thus is characterized by suppressed convection. The region of maximum suppressed convection, initially located to the west of the westerly anomaly around 15°N and -130°W , propagates slowly to the east after the passage of the MJO. This region of suppressed convection moves toward the east with relatively constant amplitude.

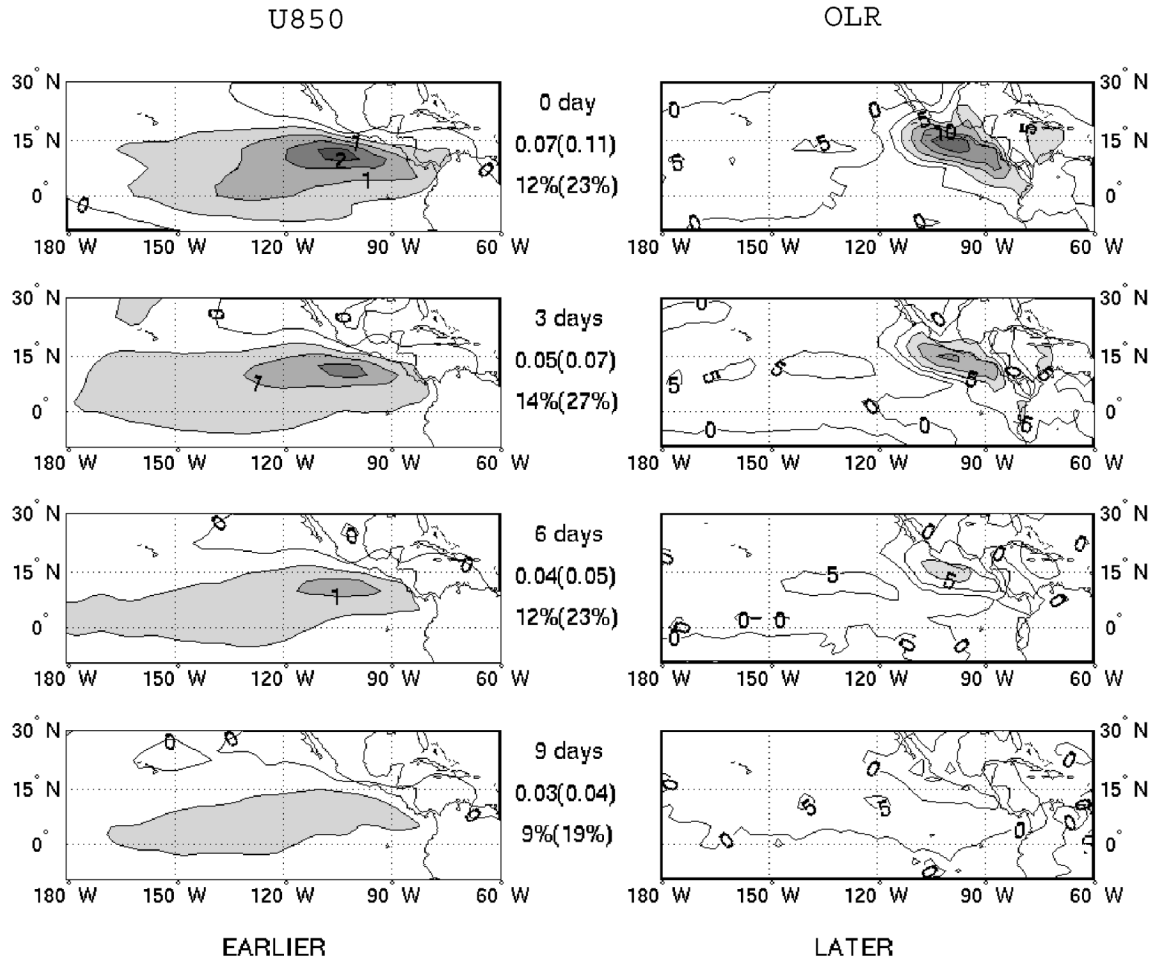


FIG. 2. LMCA of OLR with 850-mb zonal wind in which the zonal wind is leading the OLR by 0, 3, 6, and 9 days. (left) Heterogeneous maps corresponding to the 850-mb zonal wind patterns. Values greater than 0.5 m s^{-1} are shaded. (right) Heterogeneous maps corresponding to the OLR patterns. Values more negative than -5 W m^{-2} are shaded. Positive values of OLR are associated with suppressed regions of convection and negative values are associated with enhanced regions of convection.

2) OLR LEADS 850-MB WIND

Figure 3 shows the LMCA first mode analysis when the OLR leads the 850-mb zonal wind. The basic features are very similar to when wind leads OLR, except that the amplitudes are larger at longer lags. The RMSC and the fraction of explained covariance values are very similar to the values in Fig. 2 in which the wind leads the OLR and shows a relatively good relationship between the two fields. The differences between Fig. 2 and Fig. 3 suggest a slightly greater importance of the convection anomalies for the wind anomalies than the other way around.

c. EOF analyses of OLR and SST

Figure 4 shows the first EOFs of the OLR and SST data. These patterns are given for reference to show that the patterns obtained from the mixed covariance studies below are consistent with the dominant mode of vari-

ability of OLR, but that the SST patterns obtained in the covariance analysis are different from the leading EOF of SST. The fraction of explained variance by the first EOF of OLR is about 4% in the large domain and about 3 times larger in the small domain. The explained variance is low because of the large amount of small-scale, high-frequency variance in the OLR field. The EOF for OLR is consistent with that obtained in previous studies (e.g., Maloney and Hartmann 1998, 2000a) and resembles the pattern obtained in the covariance analysis with the wind field shown in Figs. 2 and 3. It shows a dipolar pattern, with one coherent region west of the westerly wind and another region roughly at the position of the westerly wind maximum (Fig. 4, left). The structures obtained from the LMCA between 850-mb zonal wind and OLR are very similar to the first EOFs of the respective fields.

The first EOF of SST, which explains 18% of the SST variance, shows mainly an extended tongue of anom-

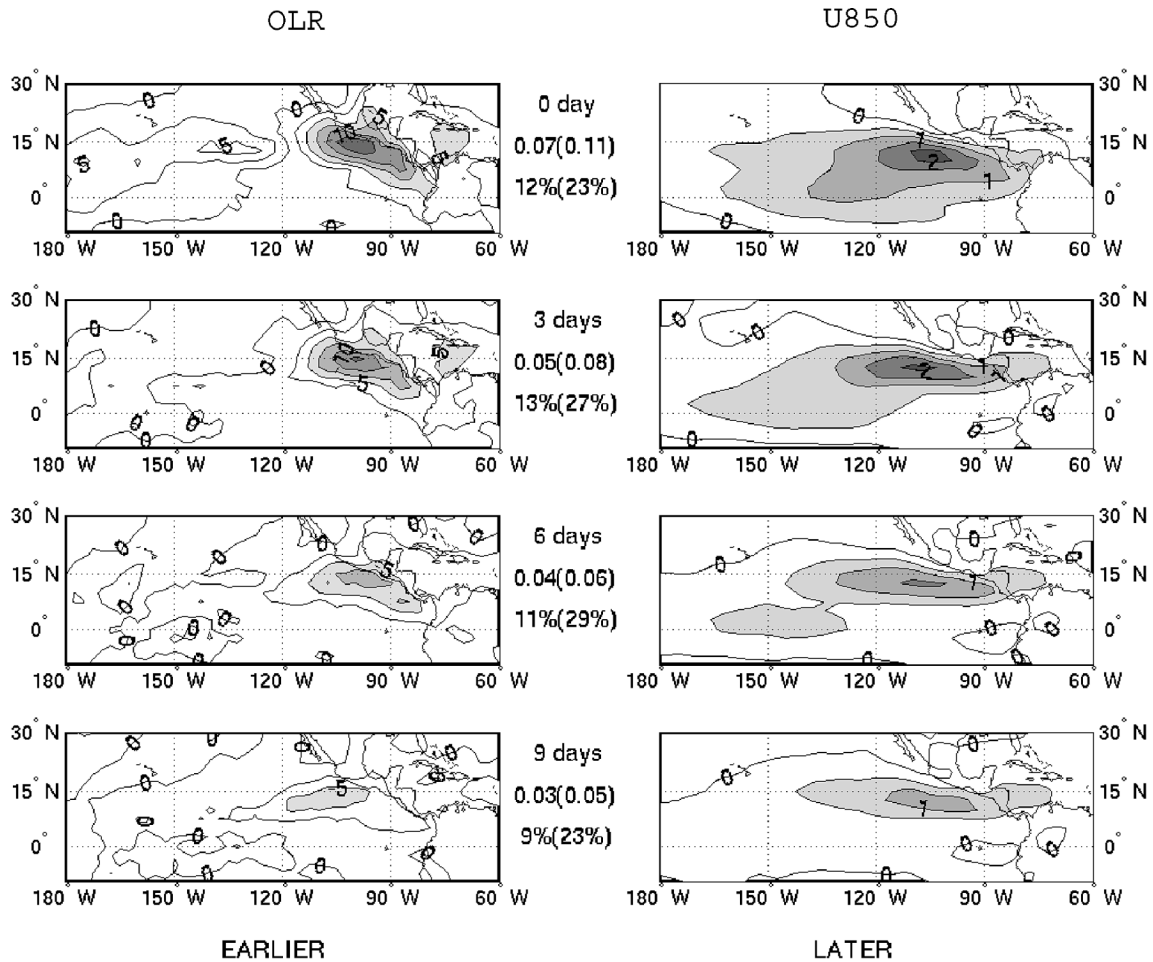


FIG. 3. Same as in Fig. 2, but for the OLR with the 850-mb zonal wind in which the OLR is leading the zonal wind by 0, 3, 6, and 9 days. (left) The OLR patterns with values more negative than $-5 W m^{-2}$ are shaded and (right) 850-mb zonal wind patterns with values greater than $0.5 m s^{-1}$ are shaded.

alous SST along the equator and no real anomalies near the coast of America (Fig. 4, right). This pattern resembles that described by Zhang (2001) and does not have the feature off the west coast of Central America that appears in modes derived from LMCA analysis between SST and OLR and SST and wind to be shown below. Zhang suggests that the equatorial SST pattern is caused by intraseasonal oceanic Kelvin waves forced by the MJO over the western/central Pacific.

d. OLR and sea surface temperature

Figure 5 shows LMCA analysis applied to the relation between OLR and SST. The explained covariance increases with increasing lag and is largest for a 9-day lag, decreases slightly for a 12-day lag, and decreases more rapidly for longer lags (not shown). Thus, the largest explained covariance occurs when SST follows OLR by between 9 and 12 days; hence, there seems to

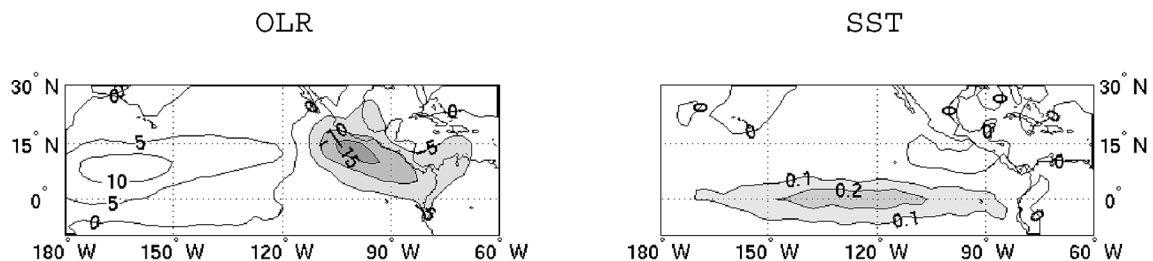


FIG. 4. (left) First EOF of OLR. Values more negative than $-5 W m^{-2}$ are shaded. (right) First EOF of SST. Values greater than $0.1 K$ are shaded.

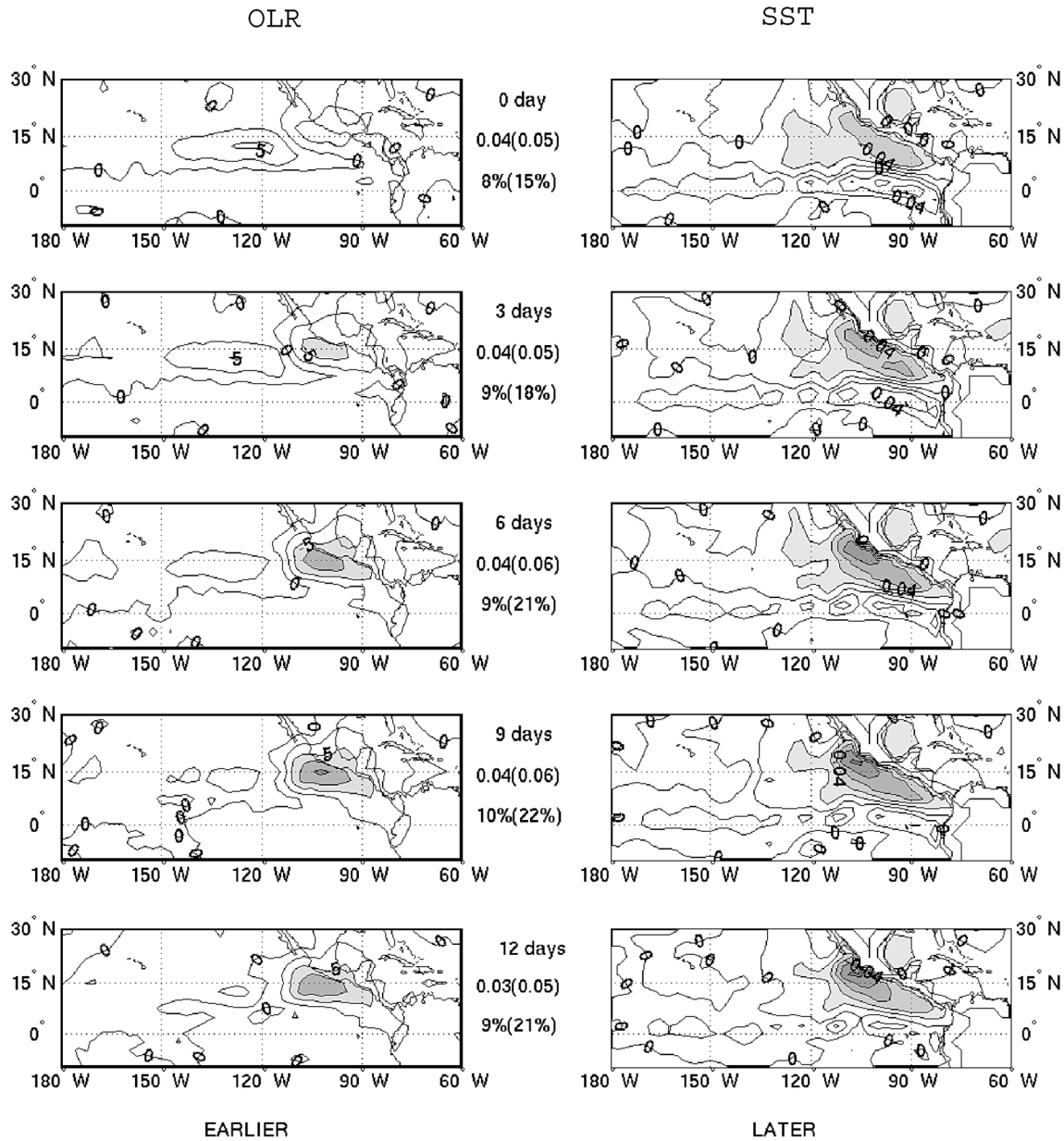


FIG. 5. Same as in Fig. 2, but for the OLR with the SST in which (left) the OLR is leading (right) the SST. Lags of 0, 3, 6, 9, and 12 are shown. OLR values more negative than -5 W m^{-2} are shaded. SST values more negative than -0.02 K are shaded.

be a lagged response of SST to convection. At this time lag, a region of enhanced convection with values of -15 W m^{-2} is followed 9 days later by a decrease of SST of about 0.1°K , in a root-mean-square sense. Individual MJO event amplitudes are in the order of 0.5 K (Maloney and Kiehl 2002a).

When the SST leads the OLR (Fig. 6), the amplitude of the pattern is not as large and does not show as significant an increase with increasing lag. Also, the fraction of explained covariance does not show as much of an increase with increasing time lag when OLR follows SST.

Figures 5 and 6 suggest a clear asymmetry in the relation between SST and OLR. Lagged covariance patterns are much stronger when OLR leads SST than vice versa. When OLR precedes SST, the amplitude explained by the first maximum covariance pattern increases with lag by a factor of 2, indicating that the covariance is stronger when low OLR anomalies west of Central America precede low SST anomalies there. When SST precedes OLR, the pattern amplitudes do not increase very much with time lag. Moreover, point-by-point correlation supports the idea that OLR drives SST much more strongly than SST drives OLR. SST leading

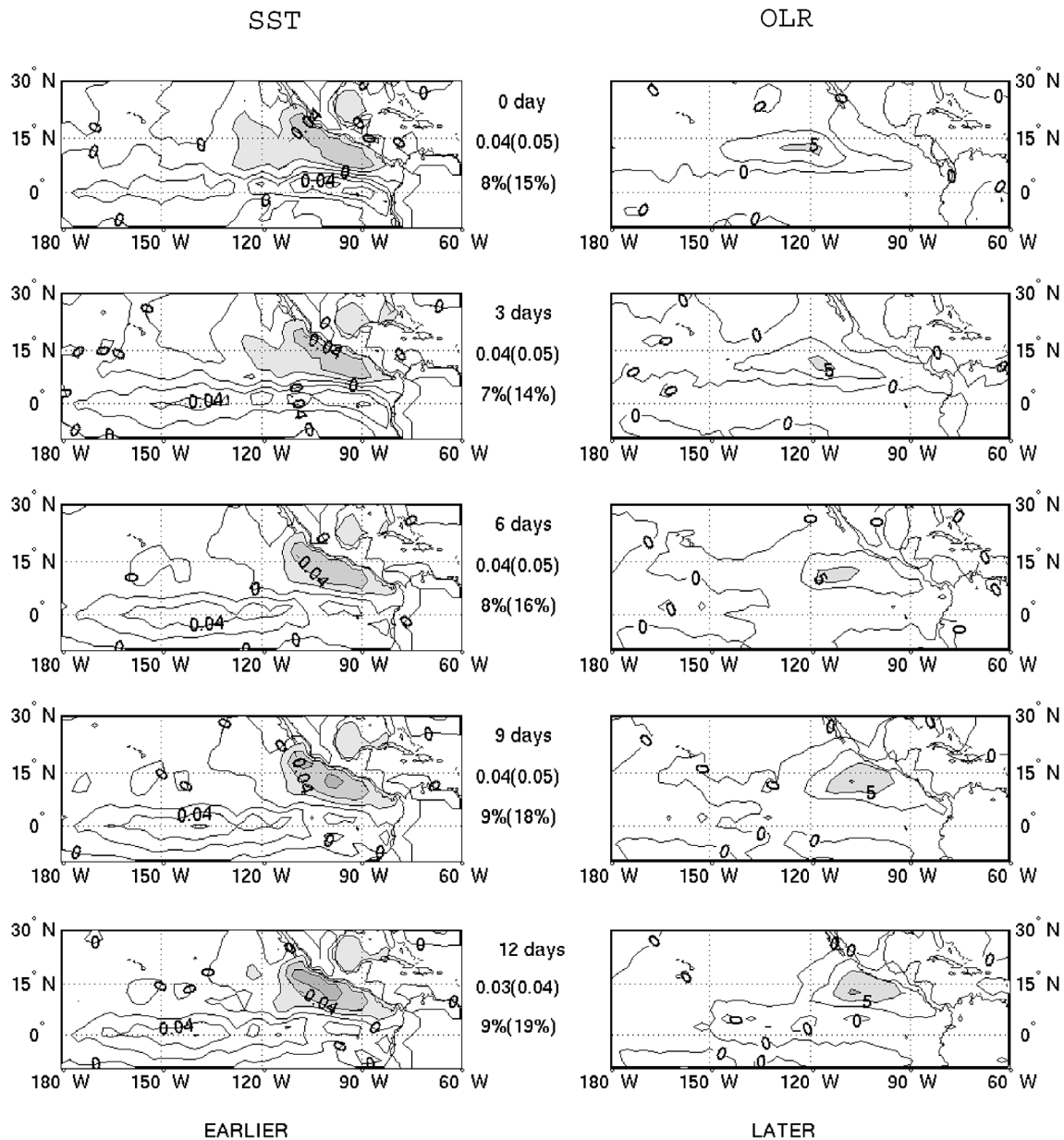


FIG. 6. Same as in Fig. 2, but for the OLR with the SST in which (left) the SST is leading (right) the OLR.

OLR by 9 days produces a correlation of about -0.1 in the area west of Central America, while OLR leading SST by 9 days produces a local correlation of about $+0.2$, a factor of 2 difference. The correlations appear small, but one must remember that high frequencies have not been removed and all the data were used.

e. 850-mb zonal wind and sea surface temperature

When the wind leads the SST, the explained covariance by the first singular vector varies in the same way as the one for OLR leading SST—the fraction of explained covariance increases with lag (Fig. 7). Explained

covariances vary between 11% and 17% for the large domain. Westerlies are followed by a decrease of SST of about 0.1°K , 9–12 days afterward.

When the SST leads the wind, less structure can be seen than when the wind leads the SST, except at zero lag. Otherwise the SST pattern does not seem to be correlated with westerlies at time lags greater than 3 days (not shown). Similarly, 850-mb zonal wind leading SST by 9 days produces a coherent pattern of correlation with maximum values greater than $+0.2$, while SST leading 850-mb zonal wind produces much smaller values of correlation. Wind and OLR variations lead coherently to SST variations on MJO time scales, but not

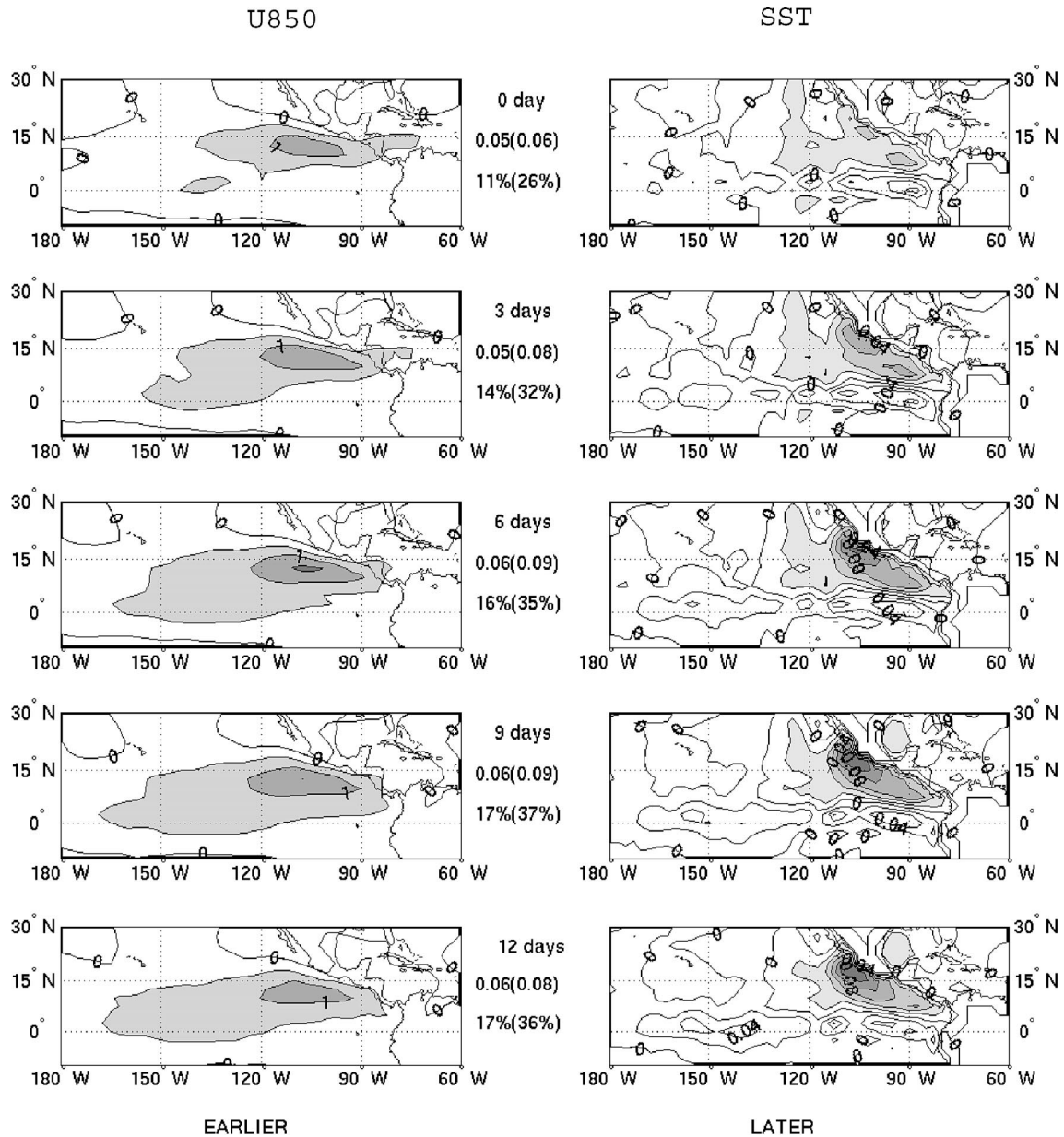


FIG. 7. Same as in Fig. 2, but for (left) the 850-mb zonal wind with (right) the SST in which the wind is leading the SST. Wind values greater than 0.5 m s^{-1} and SST values more negative than -0.02 K are shaded. Lags of 0, 3, 6, 9, and 12 are shown.

vice versa. Maloney and Kiehl (2002b) show that SST variations seem to improve the simulation of intraseasonal variability in the East Pacific in the National Center for Atmospheric Research (NCAR) Community Climate Model, version 3 (CCM3) but the mechanism whereby SST influences the MJO is not easily revealed by a lagged variance analysis.

4. Summary and conclusions

Lagged maximum covariance analysis (LMCA) was used to compute the structures that explain the maxi-

mum covariance between zonal wind, OLR, and SST in the eastern Pacific region during Northern Hemisphere summer. The zonal wind pattern at 850 mb that best explains the covariance with OLR and SST is a zonal jet that is centered near 12°N , 100°W . This pattern appears to propagate slowly from west to east and a precursor signal in the central equatorial Pacific can be seen at least 9 days before the strongest winds near the coast of Central America.

LMCA between 850-mb wind and OLR indicates that westerly wind anomalies to the west precede development of OLR anomalies near the coast of Central Amer-

ica. On the other hand, larger covariances are obtained when OLR leads 850-mb wind than when wind leads OLR. This suggests that the OLR anomalies near the coast may be triggered by zonal wind anomalies propagating from the west, but that once convection develops, it acts to locally strengthen the 850-mb westerly jet anomaly in the East Pacific.

LMCA between OLR and SST indicates that negative OLR anomalies precede negative SST anomalies in the region immediately off the coast of Central America. At lags of a week or more, covariance between OLR and SST near Central America is larger when OLR precedes SST than when SST precedes OLR, and a more coherent signal with larger amplitude is seen. This indicates that the role of convection in changing SST is larger and more coherent than the role of changed SST in modifying convection. The covariance between SST and 850-mb zonal wind is also larger when the winds precede the SST, suggesting that the westerly wind anomalies and associated convection lead to SST reductions in the region near the coast of Central America. These results suggest that the convection and associated wind anomalies drive the SST much more strongly than SST variations influence MJO wind and rainfall anomalies.

Acknowledgments. This research was supported by the NOAA CLIVAR PACS Program under Grant GC00-358 and by the Joint Institute for the Study of the Atmosphere and Ocean (JISAO) under NOAA Cooperative Agreement Number NA17RJ1232.

REFERENCES

- Bretherton, C. S., C. Smith, and J. M. Wallace, 1992: An intercomparison of methods for finding coupled patterns in climate data. *J. Climate*, **5**, 541–560.
- Gibson, J. K., P. Kallberg, S. Uppala, A. Nourmura, A. Hernandez, and E. Serrano, 1997: ERA description. ECMWF Re-Analysis Project Rep. Series 1, ECMWF, Reading, United Kingdom, 77 pp.
- Knutson, T. R., K. M. Weickmann, and J. E. Kutzbach, 1986: Global-scale intraseasonal oscillations of outgoing longwave radiation and 250 mb zonal wind during Northern Hemisphere summer. *Mon. Wea. Rev.*, **114**, 605–623.
- Liebmann, B., and C. A. Smith, 1996: Description of a complete (interpolated) outgoing longwave radiation dataset. *Bull. Amer. Meteor. Soc.*, **77**, 1275–1277.
- Madden, R. A., and P. R. Julian, 1994: Observations of the 40–50-day tropical oscillation—A review. *Mon. Wea. Rev.*, **122**, 814–837.
- Maloney, E. D., and D. L. Hartmann, 1998: Frictional moisture convergence in a composite life cycle of the Madden–Julian oscillation. *J. Climate*, **11**, 2387–2403.
- , and —, 2000a: Modulation of eastern North Pacific hurricanes by the Madden–Julian oscillation. *J. Climate*, **13**, 1451–1460.
- , and —, 2000b: Modulation of hurricane activity in the Gulf of Mexico measured by the MJO. *Science*, **287**, 2002–2004.
- , and —, 2001: The Madden–Julian oscillation, barotropic dynamics, and North Pacific tropical cyclone formation. Part I: Observations. *J. Atmos. Sci.*, **58**, 2545–2558.
- , and J. T. Kiehl, 2002a: MJO-related SST variations over the tropical eastern Pacific during Northern Hemisphere summer. *J. Climate*, **15**, 675–689.
- , and —, 2002b: Intraseasonal eastern Pacific precipitation and SST variations in a GCM coupled to a slab ocean model. *J. Climate*, **15**, 2989–3007.
- von Storch, H., and F. W. Zwiers, 1999: *Statistical Analysis in Climate Research*. Cambridge University Press, 484 pp.
- Wallace, J. M., C. Smith, and C. S. Bretherton, 1992: Singular value decomposition of wintertime sea surface temperature and 500-mb height anomalies. *J. Climate*, **5**, 561–576.
- Weickmann, K. M., 1983: Intraseasonal circulation and outgoing longwave radiation modes during Northern Hemisphere winter. *Mon. Wea. Rev.*, **111**, 1838–1858.
- , G. R. Lussky, and J. E. Kutzbach, 1985: Intraseasonal (30–60 day) fluctuations of outgoing longwave radiation and 250 mb streamfunction during northern winter. *Mon. Wea. Rev.*, **113**, 941–961.
- Zhang, C., 2001: Intraseasonal perturbation in sea surface temperature of the equatorial eastern Pacific and their association with the Madden–Julian oscillation. *J. Climate*, **14**, 1309–1322.